Open Access **Baghdad Science Journal** **P-ISSN: 2078-8665**
2021, 18(4) Supplement: 1521-1535 **E-ISSN: 2411-7986**

DOI: https://dx.doi.org/10.21123/bsj.2021.18.4(Suppl.).1521

Numerical Analysis of Least-Squares Group Finite Element Method for Coupled Burgers' Problem

Najat Jalil Noon

Department of Mathematics, College of Education for Pure Science, University of Basrah.
Email: fini.burg@gmail.com

Received 1/8/2019, Accepted 15/8/2021, Published 20/12/2021

This work is licensed under a Creative Commons Attribution 4.0 International License.

Abstract:

In this paper, a least squares group finite element method for solving coupled Burgers' problem in 2-D is presented. A fully discrete formulation of least squares finite element method is analyzed, the backward-Euler scheme for the time variable is considered, the discretization with respect to space variable is applied as biquadratic quadrangular elements with nine nodes for each element. The continuity, ellipticity, stability condition and error estimate of least squares group finite element method are proved. The theoretical results show that the error estimate of this method is $o(h^r)$. The numerical results are compared with the exact solution and other available literature when the convection-dominated case to illustrate the efficiency of the proposed method that are solved through implementation in MATLAB R2018[a].

Keywords: Burgers' problem, Group finite element method, Least square.

Introduction:

Nonlinear partial differential equations arise in many fields of science, particularly in physics and engineering [1-2]. The Burgers' equation is an important equation. It is widely used to model several physical flow phenomena in fluid dynamics teaching and in engineering. Several methods have been intensively studied to this equation, such as the least squares finite element methods. Some of the most relevant literature can be summarized, Bárbara, Roberta, Paula and Romão [3] applied the least squares finite element method for 1-D Burgers' equation with the linearization of Newton method. The numerical solution obtained was compared with the exact solution and the L^{∞}errors were calculated for this method. Konzen, Azevedo, Sauter and Zingano [4] studied the Galerkin least squares finite element method for 1-D Burgers' equation subjected to initial conditions with compact support. The numerical simulations are performed by considering a sequence of auxiliary spatially dimensionless Dirichlet's problems parameterized by its numerical support and the numerical solutions was compared with exact solutions. Ye and Zhang [5] applied the discontinuous least-squares (DLS) finite element method to second-order elliptic equations. Theoretical error estimates were presented and numerical solutions were given to demonstrate the accuracy approximate of this method. Kalchev, Manteuffel and Münzenmaier [6] studied Mixed $(\mathcal{L}\mathcal{L}^*)^{-1}$ and $(\mathcal{L}\mathcal{L}^*)$ least-squares finite element methods with application to linear hyperbolic problems. They were founded upon and extended the $\mathcal{L}\mathcal{L}^*$ approach that is rather general and applicable beyond the setting of elliptic problems. The error bounds and the factors affecting the convergence show the guarantee optimal rates.

The group finite element method (GrFEM), also known as product approximation is a finite element (FE) technique for types of nonlinear PDEs. Experiments with the GrFEM have shown an increase in economy and in the nodal accuracy compared to FE solutions of the Burgers' equations [7-9]. In this paper, the least squares group finite element method for 2-D coupled Burgers' problem with a fully-discrete approximation for the time variable is presented. The continuity, ellipticity, stability and error estimate for this method is proved. The numerical solutions are compared with the exact solution and other available solutions when the convection-dominated case to measure the numerical errors and the efficiency of our method.

Time dependent modeling problem

Consider the nonlinear time-dependent for the two dimensional coupled Burgers' problem [10],

$$u_t - \epsilon\nabla.\nabla u + u\,u_x + v\,u_y = 0, \quad \Omega \times (0,T],$$

$$v_t - \epsilon\nabla.\nabla v + u\,v_x + v\,v_y = 0, \quad \Omega \times (0,T],$$

$$u(x,y,t) = \rho_1\,, v(x,y,t) = \rho_2\,, \quad \partial\Omega \times (0,T],$$

$$u(x,y,0) = u^0(x,y), \quad v(x,y,0) = v^0(x,y)\,, \quad \overline{\Omega} \times (0,T],$$

where $\epsilon = \frac{1}{Re}$ is a viscosity constant where Re is Reynolds number, $\Omega \subset R^2$ with boundary $\partial\Omega$, $\overline{\Omega} = \Omega \cup \partial\Omega$, $T > 0$ represents the given final time and $\rho_1,\ \rho_2 \in L^2(\Omega)$. The conservation form of Burgers' equation which expresses the nonlinear terms of a PDE in grouped form is represented as following, here the $u\,u_x$ and $v\,v_y$ terms are replaced by $\frac{1}{2}(u^2)_x$ and $\frac{1}{2}(v^2)_y$ respectively,

$$u_t - \epsilon\nabla.\nabla u + \frac{1}{2}(u^2)_x + v\,u_y = 0, \quad \Omega \times (0,T], \quad \text{...1}$$

$$v_t - \epsilon\nabla.\nabla v + u\,v_x + \frac{1}{2}(v^2)_y = 0, \quad \Omega \times (0,T] \quad \text{...2}$$

$$u(x,y,t) = \rho_1\,, v(x,y,t) = \rho_2\,, \quad \partial\Omega \times (0,T],$$

$$u(x,y,0) = u^0(x,y), \quad v(x,y,0) = v^0(x,y)\,, \quad \overline{\Omega} \times (0,T],$$

The fully formulations of 1 – 2 using the finite difference approach for the time discretization such as the backward differences quotient are,

$$\frac{u^n - u^{n-1}}{k} - \epsilon\nabla.\nabla u^n + \frac{1}{2}((u^n)^2)_x + v^n\,u_y^n = 0, \quad \Omega \times (0,T],$$

$$\frac{v^n - v^{n-1}}{k} - \epsilon\nabla.\nabla v^n + u^n\,v_x^n + \frac{1}{2}((v^n)^2)_y = 0, \quad \Omega \times (0,T],$$

$$u^n(x,y,t) = \rho_1\,, \quad v^n(x,y,t) = \rho_2\,, \quad \partial\Omega \times (0,T],$$

so,

$$u^n - k\epsilon\nabla.\nabla u^n + \frac{k}{2}((u^n)^2)_x + k\,v^n\,u_y^n = f, \quad \Omega \times (0,T], \quad \text{...3}$$

$$v^n - k\epsilon\nabla.\nabla v^n + k\,u^n\,v_x^n + \frac{k}{2}((v^n)^2)_y = g, \quad \Omega \times (0,T] \quad \text{...4}$$

$$u^n(x,y,t) = \rho_1\,, v^n(x,y,t) = \rho_2\,, \partial\Omega \times (0,T],$$

where, $f = u^{n-1}$, $g = v^{n-1}$ and $k = t^n - t^{n-1}$ is the time step.

Least - squares finite element method (LSGrFEM)

In this section, the least-squares functional will be defined and proved the continuity and ellipticity for it, then the LSGrFEM for the problem 3-4 will be derived. The least-squares functional is defined as the following [11],

$$\mathcal{F}_1(\varphi, f) = \left\| \varphi - k\epsilon\nabla.\nabla\varphi + \frac{k}{2}(\varphi^2)_x + k\psi\varphi_y - f \right\|^2, \quad \text{...5}$$

$$\mathcal{F}_2(\psi, g) = \left\| \psi - k\epsilon\nabla.\nabla\psi + k\varphi\psi_x + \frac{k}{2}(\psi^2)_y - g \right\|^2, \quad \forall\ \varphi, \psi \in H^1(\Omega)\,. \quad \text{...6}$$

Lemma 1. $\mathcal{F}_1(\varphi, 0)$ and $\mathcal{F}_2(\psi, 0)$ given by 5-6 are continuous.

Proof. Note that،

$$\mathcal{F}_1(\varphi, 0) = \left\| \varphi - k\epsilon\nabla.\nabla\varphi + \frac{k}{2}(\varphi^2)_x + k\psi\varphi_y \right\|^2,$$

$$\mathcal{F}_2(\psi, 0) = \left\| \psi - k\epsilon\nabla.\nabla\psi + k\varphi\psi_x + \frac{k}{2}(\psi^2)_y \right\|^2,$$

by triangle and Cauchy Schwartz's inequalities،

$$\mathcal{F}_1(\varphi, 0) \le \left(\|\varphi\| - k\epsilon\|\nabla.\nabla\varphi\| + \frac{k}{2}\|(\varphi^2)_x\| + k\|\psi\|\|\varphi_y\| \right)^2,$$

$$\mathcal{F}_2(\psi, 0) \le \left(\|\psi\| - k\epsilon\|\nabla.\nabla\psi\| + k\|\varphi\|\|\psi_x\| + \frac{k}{2}\|(\psi^2)_y\| \right)^2,$$

by Young's inequality and the inverse estimate [12],

$$\mathcal{F}_1(\varphi, 0) \le C\left\{ \|\varphi\|^2 - \epsilon\|\nabla\varphi\|^2_{L^\infty\left(H^1(\Omega)\right)} + \frac{1}{2}\|\varphi\|^2_{L^\infty\left(H^1(\Omega)\right)} + \|\psi\|^2 + \|\varphi_y\|^2 \right\} \le C_1\{\|\varphi\|_1^2 + \|\psi\|_1^2\}, \quad \text{...7}$$

$$\mathcal{F}_2(\varphi, 0) \le C\left\{ \|\psi\|^2 - \epsilon\|\nabla\psi\|^2_{L^\infty\left(H^1(\Omega)\right)} + \|\varphi\|^2 + \|\psi_x\|^2 + \frac{1}{2}\|\psi\|^2_{L^\infty\left(H^1(\Omega)\right)} \right\} \le C_2\{\|\varphi\|_1^2 + \|\psi\|_1^2\} \quad \text{...8}$$

Lemma 2. $\mathcal{F}_1(\varphi, 0)$ and $\mathcal{F}_2(\psi, 0)$ given by 5-6 are V-elliptic.

Proof. Note that،

$$\left(\varphi+\frac{k}{2}(\varphi^2)_x+k\psi\varphi_y\,,\varphi\right)=$$

$$\left(\varphi-k\epsilon\nabla.\nabla\varphi+\frac{k}{2}(\varphi^2)_x+k\psi\varphi_y\,,\varphi\right)+(k\epsilon\nabla.\nabla\varphi\,,\varphi),$$

$$\left(\psi+k\varphi\psi_x+\tfrac{k}{2}(\psi^2)_y\,,\psi\right)=\left(\psi-k\epsilon\nabla.\nabla\psi+k\varphi\psi_x+\tfrac{k}{2}(\psi^2)_y\,,\psi\right)+(k\epsilon\nabla.\nabla\psi\,,\psi),$$

by Cauchy Schwartz's inequality,

$$\left(\|\varphi\|+\tfrac{k}{2}\|(\varphi^2)_x\|+k\left\|\psi\varphi_y\right\|\right)\|\varphi\|\leq\left(\left\|\varphi-k\epsilon\nabla.\nabla\varphi+\tfrac{k}{2}(\varphi^2)_x+k\psi\varphi_y\right\|+\|k\epsilon\nabla.\nabla\varphi\|\right)\|\varphi\|,$$

$$\left(\|\psi\|+k\|\varphi\psi_x\|+\tfrac{k}{2}\left\|(\psi^2)_y\right\|\right)\|\psi\|\leq\left(\left\|\psi-k\epsilon\nabla.\nabla\psi+k\varphi\psi_x+\tfrac{k}{2}(\psi^2)_y\right\|+\|k\epsilon\nabla.\nabla\psi\|\right)\|\psi\|,$$

from 5 and 6 note that,

$\|k\epsilon\nabla.\nabla\varphi\|\leq\mathcal{F}_1^{\frac{1}{2}}(\varphi,0)$ and $\|k\epsilon\nabla.\nabla\psi\|\leq\mathcal{F}_2^{\frac{1}{2}}(\psi,0)$, so that,

$$\|\varphi\|+\tfrac{k}{2}\|(\varphi^2)_x\|+k\left\|\psi\varphi_y\right\|\leq\left\|\varphi-k\epsilon\nabla.\nabla\varphi+\tfrac{k}{2}(\varphi^2)_x+k\psi\varphi_y\right\|+\mathcal{F}_1^{\frac{1}{2}}(\varphi,0),$$

$$\|\psi\|+k\|\varphi\psi_x\|+\tfrac{k}{2}\left\|(\psi^2)_y\right\|\leq\left\|\psi-k\epsilon\nabla.\nabla\psi+k\varphi\psi_x+\tfrac{k}{2}(\psi^2)_y\right\|+\mathcal{F}_2^{\frac{1}{2}}(\psi,0),$$

so,

$$\|\varphi\|+\tfrac{k}{2}\|(\varphi^2)_x\|+k\left\|\psi\varphi_y\right\|\leq 2\mathcal{F}_1^{\frac{1}{2}}(\varphi,0),$$

$$\|\psi\|+k\|\varphi\psi_x\|+\tfrac{k}{2}\left\|(\psi^2)_y\right\|\leq 2\mathcal{F}_2^{\frac{1}{2}}(\psi,0),$$

thus,

$$\mathcal{F}_1(\varphi,0)\geq C_3\{\|\varphi\|_1^2+\|\psi\|_1^2\}\,, \qquad \textbf{...9}$$

$$\mathcal{F}_2(\psi,0)\geq C_4\{\|\varphi\|_1^2+\|\psi\|_1^2\}\,. \qquad \textbf{...10}$$

Where, C, C_1, C_2, C_3 and C_4 are positive constants. The necessary condition so that the exact solutions $u\,, v\in H^1\,(\Omega)$ of problem 3-4 be the zero minimizer of the functional $\mathcal{F}_1$ and $\mathcal{F}_2$ respectively are,

$$\mathcal{F}_1(u^n,f)=0=min\{\mathcal{F}_1(\varphi,f):\ \varphi\in H^1\,(\Omega)\},$$

$$\mathcal{F}_2(v^n,\ g)=0=min\{\mathcal{F}_2(\psi,g):\ \psi\in H^1\,(\Omega)\}.$$

Since $\mathcal{F}_1(u^n+\delta_1\varphi,f)$ and $\mathcal{F}_2(v^n+\delta_2\psi,g)$ are nonnegative quadratic functional in the variables $\delta_1,\,\delta_2\in R$ for any given $\varphi,\ \psi\in H^1\,(\Omega)$, then,

$$\frac{d}{d\delta_1}\mathcal{F}_1(u^n,f)|_{\delta_1=0}\ =0\,,$$

$$\frac{d}{d\delta_2}\mathcal{F}_2(v^n,g)|_{\delta_2=0}\ =0\,,$$

which are equivalent to,

$$\beta_1(u^n,\varphi)=\ell_1(\varphi), \qquad \textbf{...11}$$

$$\beta_2(v^n,\psi)=\ell_2(\psi), \qquad \textbf{...12}$$

where,

$$\beta_1(u^n,\varphi)=\int_\Omega\left(u^n-k\epsilon\nabla.\nabla u^n+\frac{k}{2}((u^n)^2)_x+kv^nu_y^n\right).\left(\varphi-k\epsilon\nabla.\nabla\varphi+\frac{k}{2}(\varphi^2)_x+k\psi\varphi_y\right)d\Omega,$$

$$\beta_2(v^n,\psi)=\int_\Omega\left(v^n-k\epsilon\nabla.\nabla v^n+ku^nv_x^n+\frac{k}{2}((v^n)^2)_y\right).\left(\psi-k\epsilon\nabla.\nabla\psi+k\varphi\psi_x+\frac{k}{2}(\psi^2)_y\right)d\Omega\,,$$

$$\ell_1(\varphi)=\int_\Omega f.\left(\varphi-k\epsilon\nabla.\nabla\varphi+\frac{k}{2}(\varphi^2)_x+k\psi\varphi_y\right)d\Omega,$$

$$\ell_2(\psi)=\int_\Omega\ g.\left(\psi-k\epsilon\nabla.\nabla\psi+k\varphi\psi_x+\frac{k}{2}(\psi^2)_y\right)d\Omega\,.$$

Note the following identities,

$$\beta_1(\varphi,\varphi)=\mathcal{F}_1(\varphi,0)=\left\|\varphi-k\epsilon\nabla.\nabla\varphi+\frac{k}{2}(\varphi^2)_x+k\psi\varphi_y\right\|^2\,,$$

$$\beta_2(\psi,\psi)=\mathcal{F}_2(\psi,0)=\left\|\psi-k\epsilon\nabla.\nabla\psi+k\varphi\psi_x+\frac{k}{2}(\psi^2)_y\right\|^2\,, \qquad \forall\varphi,\ \psi\in H^1\,(\Omega)\,.$$

Now, the finite dimensional space $V_h\subset H^1\,(\Omega)$ is defined, such that the following inequalities will be held, for some integer $s\geq 2$ and small h (where h denotes the grid size of our triangulations of the domain $\overline{\Omega}$) and for any $\varphi,\ \psi\in H^r\,(\Omega)$ there exist $\varphi_h,\ \psi_h\in V_h^r$,

$$\|\varphi-\varphi_h\|_0+h\|\varphi-\varphi_h\|_1\leq Ch^r\|\varphi\|_r\,, \qquad \textbf{...13}$$

$$\|\psi-\psi_h\|_0+h\|\psi-\psi_h\|_1\leq Ch^r\|\psi\|_r\,,$$

$$1\leq r\leq s \quad \textbf{...14}$$

The LSGrFEM for 3- 4 is defined as: find u_h, $v_h \in V_h$ the approximation solution of u and v respectively such that,

$$\beta_1(u_h^n, \varphi_h) = \ell_1(\varphi_h), \quad \ldots 15$$

$$\beta_2(v_h^n, \psi_h) = \ell_2(\psi_h). \quad \ldots 16$$

Stability and error estimate. Let $u^n, v^n \in H^1(\Omega)$ and u_h^n , $v_h^n \in V_h$ denote the solutions of problems 3 – 4 and 15 - 16, respectively. Since $V_h \subset H^1(\Omega)$, by using the equations in 11 - 12 and 15 – 16 , the following orthogonality relations are obtained :

$$\beta_1(u^n - u_h^n, \varphi_h) = 0, \quad \ldots 17$$

$$\beta_2(v^n - v_h^n, \psi_h) = 0, \ \forall \ \varphi_h \ , \ \psi_h \in V_h \ . \quad \ldots 18$$

From 17 – 18 and by using Cauchy Schwarz's inequality then,

$$\begin{aligned}
&\left\|\left(u^n - k\epsilon\nabla.\nabla u^n + \frac{k}{2}((u^n)^2)_x + kv^n u_y^n\right)\right. \\
&\qquad - \left(u_h^n - k\epsilon\nabla.\nabla u_h^n + \frac{k}{2}((u_h^n)^2)_x\right. \\
&\qquad \left.\left. + kv_h^n(u_h^n)_y\right)\right\|^2 \\
&\qquad = \ \beta_1(u^n - u_h^n, u^n - u_h^n) \\
&\qquad = \ \beta_1(u^n - u_h^n, u^n - \varphi_h)
\end{aligned}$$

$$\begin{aligned}
\leq &\left\|\left(u^n - k\epsilon\nabla.\nabla u^n + \frac{k}{2}((u^n)^2)_x + kv^n u_y^n\right)\right. \\
&\qquad - \left(u_h^n - k\epsilon\nabla.\nabla u_h^n + \frac{k}{2}((u_h^n)^2)_x\right. \\
&\qquad \left.\left. + kv_h^n(u_h^n)_y\right)\right\|^2 . \left\|\left(u^n - k\epsilon\nabla.\nabla u^n\right.\right. \\
&\qquad \left. + \frac{k}{2}((u^n)^2)_x + kv^n u_y^n\right) \\
&\qquad - \left(\varphi_h - k\epsilon\nabla.\nabla\varphi_h + \frac{k}{2}((\varphi_h)^2)_x\right. \\
&\qquad \left.\left. + k\psi_h(\varphi_h)_y\right)\right\|^2 ,
\end{aligned}$$

$$\begin{aligned}
&\left\|\left(v^n - k\epsilon\nabla.\nabla v^n + ku^n v_x^n + \frac{k}{2}((v^n)^2)_y\right)\right. \\
&\qquad - \left(v_h^n - k\epsilon\nabla.\nabla v_h^n + ku_h^n(v_h^n)_x\right. \\
&\qquad \left.\left. + \frac{k}{2}((v_h^n)^2)_y\right)\right\|^2 \\
&\qquad = \ \beta_2(v^n - v_h^n, v^n - v_h^n) \\
&\qquad = \ \beta_2(v^n - v_h^n, v^n - \psi_h)
\end{aligned}$$

$$\begin{aligned}
\leq &\left\|\left(v^n - k\epsilon\nabla.\nabla v^n + ku^n v_x^n + \frac{k}{2}((v^n)^2)_y\right)\right. \\
&\qquad - \left(v_h^n - k\epsilon\nabla.\nabla v_h^n + ku_h^n(v_h^n)_x\right. \\
&\qquad \left. + \frac{k}{2}((v_h^n)^2)_y\right)\Big\|^2 . \left\|\left(v^n\right.\right. \\
&\qquad - k\epsilon\nabla.\nabla v^n + ku^n v_x^n \\
&\qquad \left. + \frac{k}{2}((v^n)^2)_y\right) \\
&\qquad - \left(\psi_h - k\epsilon\nabla.\nabla\psi_h + k\varphi_h(\psi_h)_x\right. \\
&\qquad \left.\left. + \frac{k}{2}((\psi_h)^2)_y\right)\right\|^2 ,
\end{aligned}$$

which implies,

$$\begin{aligned}
&\left\|\left(u^n - k\epsilon\nabla.\nabla u^n + \tfrac{k}{2}((u^n)^2)_x + \right.\right. \\
&\left.\left. kv^n u_y^n\right) - \left(u_h^n - k\epsilon\nabla.\nabla u_h^n + \tfrac{k}{2}((u_h^n)^2)_x + \right.\right. \\
&\left.\left. kv_h^n(u_h^n)_y\right)\right\| \leq \ \left\|\left(u^n - k\epsilon\nabla.\nabla u^n + \right.\right. \\
&\left.\left. \tfrac{k}{2}((u^n)^2)_x + kv^n u_y^n\right) - \left(\varphi_h - k\epsilon\nabla.\nabla\varphi_h + \right.\right. \\
&\left.\left. \tfrac{k}{2}((\varphi_h)^2)_x + k\psi_h(\varphi_h)_y\right)\right\| , \quad \ldots 19
\end{aligned}$$

$$\begin{aligned}
&\left\|\left(v^n - k\epsilon\nabla.\nabla v^n + ku^n v_x^n + \right.\right. \\
&\left.\left. \tfrac{k}{2}((v^n)^2)_y\right) - \left(v_h^n - k\epsilon\nabla.\nabla v_h^n + \right.\right. \\
&\left.\left. ku_h^n(v_h^n)_x + \tfrac{k}{2}((v_h^n)^2)_y\right)\right\| \leq \ \left\|\left(v^n - \right.\right. \\
&\left.\left. k\epsilon\nabla.\nabla v^n + ku^n v_x^n + \tfrac{k}{2}((v^n)^2)_y\right) - \right. \\
&\left.\left(\psi_h - k\epsilon\nabla.\nabla\psi_h + k\varphi_h(\psi_h)_x + \right.\right. \\
&\left.\left. \tfrac{k}{2}((\psi_h)^2)_y\right)\right\| . \quad \ldots 20
\end{aligned}$$

Theorem 1. The method described by 15 – 16 is stable over finite time, specifically, for any $N > 0$,

$$\|u_h^N\| \leq \|u_h^0\| ,$$

$$\|v_h^N\| \leq \|v_h^0\| .$$

Proof. Note that,

$$\beta_1(u_h^n, u_h^n) = \ell_1(u_h^n) ,$$

$$\beta_2(v_h^n, v_h^n) = \ell_2(v_h^n) ,$$

$$\begin{aligned}
&\left\|u_h^n - k\epsilon\nabla.\nabla u_h^n + \frac{k}{2}(u_h^n)^2)_x + kv_h^n(u_h^n)_y\right\|^2 \\
&\qquad = \ell_1(u_h^n) ,
\end{aligned}$$

$$\begin{aligned}
&\left\|v_h^n - k\epsilon\nabla.\nabla v_h^n + ku_h^n(v_h^n)_x + \frac{k}{2}(v_h^n)^2)_y\right\|^2 \\
&\qquad = \ell_2(v_h^n) ,
\end{aligned}$$

by Cauchy Schwartz's inequality then,

$$\left\|u_h^n - k\epsilon\nabla.\nabla u_h^n + \frac{k}{2}(u_h^n)^2)_x + kv_h^n(u_h^n)_y\right\|^2 \le \|f_h\|.\left\|u_h^n - k\epsilon\nabla.\nabla u_h^n + \frac{k}{2}(u_h^n)^2)_x + kv_h^n(u_h^n)_y\right\|,$$

$$\left\|u_h^n - k\epsilon\nabla.\nabla u_h^n + \frac{k}{2}(u_h^n)^2)_x + kv_h^n(u_h^n)_y\right\|^2 \le \|g_h\|.\left\|v_h^n - k\epsilon\nabla.\nabla v_h^n + ku_h^n(v_h^n)_x + \frac{k}{2}(v_h^n)^2)_y\right\|,$$

from the V-elliptic of the bilinear form of Lemma 2 then,

$$\|u_h^n\| \le \|f_h\|,$$

$$\|v_h^n\| \le \|g_h\|,$$

summing both sides from $n = 1$ to $n = N$ to get the following,

$$\|u_h^N\| \le \|u_h^0\|,$$

$$\|v_h^N\| \le \|v_h^0\|.$$

Theorem 2. Let C_7 and C_8 are positive constants independent of h then the following error estimates are hold :

$$\max_{1\le n\le N}\|u^n - u_h^n\| \le C_7 h^r \max_{1\le n\le N}\|u^n\|_r,$$

$$\max_{1\le n\le N}\|v^n - v_h^n\| \le C_8 h^r \max_{1\le n\le N}\|v^n\|_r.$$

Proof. From 9 - 10, 19 - 20 and 7 – 8 then,

$$\|u^n - u_h^n\| \le \left\|\left(u^n - k\epsilon\nabla.\nabla u^n + \frac{k}{2}((u^n)^2)_x + kv^n u_y^n\right) - \left(u_h^n - k\epsilon\nabla.\nabla u_h^n + \frac{k}{2}((u_h^n)^2)_x + kv_h^n(u_h^n)_y\right)\right\| \le \left\|\left(u^n - k\epsilon\nabla.\nabla u^n + \frac{k}{2}((u^n)^2)_x + kv^n u_y^n\right) - \left(\varphi_h - k\epsilon\nabla.\nabla\varphi_h + \frac{k}{2}((\varphi_h)^2)_x + k\psi_h(\varphi_h)_y\right)\right\| \le C_5\|u^n - \varphi_h\|,$$

$$\|v^n - v_h^n\| \le \left\|\left(v^n - k\epsilon\nabla.\nabla v^n + ku^n v_x^n + \frac{k}{2}((v^n)^2)_y\right) - \left(v_h^n - k\epsilon\nabla.\nabla v_h^n + ku_h^n(v_h^n)_x + \frac{k}{2}((v_h^n)^2)_y\right)\right\| \le \left\|\left(v^n - k\epsilon\nabla.\nabla v^n + ku^n v_x^n + \frac{k}{2}((v^n)^2)_y\right) - \left(\psi_h - k\epsilon\nabla.\nabla\psi_h + k\varphi_h(\psi_h)_x + \frac{k}{2}((\psi_h)^2)_y\right)\right\| \le C_6\|v^n - \psi_h\|,$$

where C_5 and C_6 are positive constants independent of h. For any $\varphi_h, \psi_h \in V_h$ choosing them such that the approximation properties 13 – 14 are satisfied, when φ and ψ are replaced by u^n and v^n then,

$$\|u^n - u_h^n\| \le C_7\, h^r\|u^n\|_r,$$

$$\|v^n - v_h^n\| \le C_8\, h^r\|v^n\|_r,$$

which imply,

$$\max_{1\le n\le N}\|u^n - u_h^n\| \le C_7 h^r \max_{1\le n\le N}\|u^n\|_r,$$

$$\max_{1\le n\le N}\|v^n - v_h^n\| \le C_8 h^r \max_{1\le n\le N}\|v^n\|_r.$$

The formulation of LSGrFEM

In this section, the formulation of LSGrFEM 15 – 16 is considered , for the convection terms $\frac{1}{2}((u_h^n)^2)_x + v_h^n(u_h^n)_y$ and $u_h^n(v_h^n)_x + \frac{1}{2}((v_h^n)^2)_y$ one can linearize them by using the simple substitution [13],

$$\frac{1}{2}((u_h^n)^2)_x + v_h^n(u_h^n)_y \cong \frac{1}{2}\left(u_h^{n-1}\,u_h^n\right)_x + v_h^{n-1}(u_h^n)_y = \frac{1}{2}\,u_h^{n-1}(\,u_h^n)_x + v_h^{n-1}(u_h^n)_y,$$

$$u_h^n(v_h^n)_x + + \frac{1}{2}((v_h^n)^2)_y \cong u_h^{n-1}(v_h^n)_x + \frac{1}{2}\left(v_h^{n-1}\,v_h^n\right)_y = u_h^{n-1}(v_h^n)_x + \frac{1}{2}v_h^{n-1}(\,v_h^n)_y,$$

where u_h^{n-1} and v_h^{n-1} are stem from the previous time step, provided u_h, $(u_h)_x$, $(u_h)_y$, v_h, $(v_h)_x$ and $(v_h)_y$ are continuous on $[0,T]$ for all $x, y \in \Omega$, and k is small enough, the approximate solutions u_h^n and v_h^n in 15 – 16 might be written in the form,

$$u_h = \sum_{j=1}^N a_j^n(t)\phi_j(x,y),$$

and

$$v_h = \sum_{j=1}^N \bar{a}_j^n(t)\phi_j(x,y).$$

From 15 - 16, the residues $\Re_1$ and $\Re_2$ can be defined as follow:

$$\Re_1 = \sum_{j=1}^N a_j^n(t)\phi_j(x,y) - k\epsilon\sum_{j=1}^N a_j^n(t)\,\nabla.\nabla\phi_j(x,y) + \tfrac{k}{2}u_h^{n-1}\sum_{j=1}^N a_j^n(t)(\phi_j(x,y))_x + k\,v_h^{n-1}\sum_{j=1}^N a_j^n(t)\left(\phi_j(x,y)\right)_y - f_h, \quad \textbf{...21}$$

$$\Re_2 = \sum_{j=1}^N \bar{a}_j^n(t)\phi_j(x,y) - k\epsilon\sum_{j=1}^N \bar{a}_j^n(t)\,\nabla.\nabla\phi_j(x,y) + k\,u_h^{n-1}\sum_{j=1}^N \bar{a}_j^n(t)(\phi_j(x,y))_x + k\,v_h^{n-1}\sum_{j=1}^N \bar{a}_j^n(t)\left(\phi_j(x,y)\right)_y - g_h. \quad \textbf{...22}$$

Baghdad Science Journal
P-ISSN: 2078-8665
E-ISSN: 2411-7986

In this method the ith weight function can be expressed as,

$$\varphi_i(x,y) = \frac{\partial \Re_1}{\partial a_i} \quad , \qquad \ldots 23$$

$$\psi_i(x,y) = \frac{\partial \Re_2}{\partial \bar{a}_i} \quad , \qquad \ldots 24$$

substituting 21 - 22 and 23 - 24 in 15 - 16 the following weighted integral is yielded,

$$\int_\Omega \Big(\sum_{j=1}^N a_j^n(t)\phi_j(x,y) - k\epsilon \sum_{j=1}^N a_j^n(t)\,\nabla.\nabla\phi_j(x,y) + \tfrac{k}{2} u_h^{n-1} \sum_{j=1}^N a_j^n(t)(\phi_j(x,y))_x + k\, v_h^{n-1} \sum_{j=1}^N a_j^n(t)\Big(\phi_j(x,y)\Big)_y\Big).\Big(\phi_i(x,y) - k\epsilon\nabla.\nabla\phi_i(x,y) + \tfrac{k}{2} u_h^{n-1}(\phi_i(x,y))_x + k\, v_h^{n-1}\big(\phi_i(x,y)\big)_y\Big)\, d\Omega = \int_\Omega f_h.\Big(\phi_i(x,y) - k\epsilon\nabla.\nabla\phi_i(x,y) + \tfrac{k}{2} u_h^{n-1}(\phi_i(x,y))_x + k\, v_h^{n-1}\big(\phi_i(x,y)\big)_y\Big)\, d\Omega \quad , \qquad \ldots 25$$

$$\int_\Omega \Big(\sum_{j=1}^N \bar{a}_j^n(t)\phi_j(x,y) - k\epsilon \sum_{j=1}^N \bar{a}_j^n(t)\,\nabla.\nabla\phi_j(x,y) + k\, u_h^{n-1} \sum_{j=1}^N \bar{a}_j^n(t)(\phi_j(x,y))_x + k\, v_h^{n-1} \sum_{j=1}^N \bar{a}_j^n(t)\Big(\phi_j(x,y)\Big)_y\Big).\Big(\phi_i(x,y) - k\epsilon\nabla.\nabla\phi_i(x,y) + k\, u_h^{n-1}(\phi_i(x,y))_x + k\, v_h^{n-1}\big(\phi_i(x,y)\big)_y\Big)\, d\Omega = \int_\Omega g_h.\Big(\phi_i(x,y) - k\epsilon\nabla.\nabla\phi_i(x,y) + k\, u_h^{n-1}(\phi_i(x,y))_x + k\, v_h^{n-1}\big(\phi_i(x,y)\big)_y\Big)\, d\Omega \,, \qquad \ldots 26$$

for $i = 1,2,\ldots\ldots,N$.

Discretisation of the domain $\bar{\Omega}$. A bounded polygonal domain $\bar{\Omega}$ is considered, the discretization is applied as biquadratic quadrangular elements with nine nodes for each element as shown in Fig. 1, in the numerical integration, the integration rule with 3×3 Gaussian integration resulting nine integration points for each element is adopted .

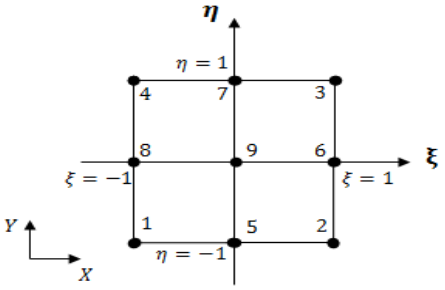

Figure 1. Nine-node isoparametric element.

The numerical results

It is well known that for $\epsilon << h$ the Burgers' equation become convection dominated case, such case makes the standard finite elements method lose stability and produce an oscillating solutions. In this section three test examples are considered to illustrate a LSGrFEM 25- 26 with $\epsilon << h$ and compare our results of the proposed method with the exact solutions and some other literature to show the accuracy and computational efficiency of our method (LSGrFEM).

Example 1. In this example, a LSGrFEM 25 – 26 over the domain $\bar{\Omega} = [0,1] \times [0,1]$ is constructed. This example has been considered in literature [14-15]. In Tab.1 the maximum errors of u and v for different grid of size at $T = 0.4$, $T = 0.8$ and $\epsilon = \frac{1}{100}$ with those obtained in literature [14] are compared. From tabular illustrations, note that, our results are better than that obtained in literature [14], also numerical solution at $h = \frac{1}{14}$, $T = 0.2$ and $k = 0.01$ for grid of size 15×15 have been shown in Fig. 2, which illustrates a better agreement than that obtained in literature [14] (Figs. 2-3). In Tab.2 for various nodes of the grid the numerical solutions at $\epsilon = \frac{1}{500}$, $h = \frac{1}{20}$, $T = 2$ and $k = 0.01$ are computed for grid of size 21×21, in tabular illustrations, our numerical results with the exact solutions and the solutions available in literature [15] are compared. It can be seen that the LSGrFEM performed better results and agreed with exact solutions than that suggested by literature [15], for which the exact solution is given as,

$$u(x,y,t) = \frac{3}{4} - \frac{1}{4\left[1+e^{\frac{-4x+4y-t}{32\epsilon}}\right]},$$

$$v(x,y,t) = \frac{3}{4} + \frac{1}{4\left[1+e^{\frac{-4x+4y-t}{32\epsilon}}\right]} \quad .$$

Numerical results are shown in Figs. 3-4. In Fig. 5, a numerical results at $\epsilon = \frac{1}{500}$, $h = \frac{1}{20}$, $T = 0.5$ and $k = 0.01$ for grid of size 21×21 are represented, note that, our method illustrate better results and agree with exact solutions than that obtained in literature [15] (Figs.1-2). From tabular illustrations and numerical results, our method gives better results and produces stable solutions than those suggested in literature [14]- [15].

Table 1. The errors $\|u-u_h\|_\infty$ and $\|v-v_h\|_\infty$ for example 1 at $\epsilon=\frac{1}{100}$ and $k=0.01$.

			$T=0.4$			
	LSGrFEM			Literature [14]		
Node size	9×9	15×15	19×19	10×10	15×15	20×20
u	0.004265	0.002040	0.001360	0.050232	0.006986	0.002136
v	0.004265	0.002040	0.001360	0.022614	0.005418	0.002554
			$T=0.8$			
u	0.005140	0.002387	0.001584	0.041652	0.003643	0.002136
v	0.005140	0.002387	0.001584	0.017284	0.004472	0.002554

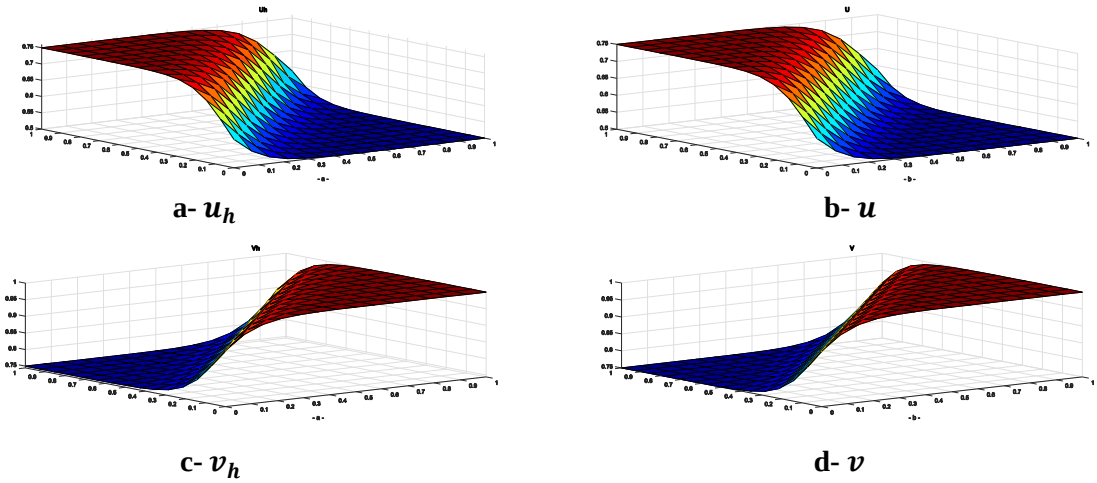

a- u_h b- u

c- v_h d- v

Figure 2. Numerical solutions of LSGrFEM and exact solutions of u and v respectively at $\epsilon=\frac{1}{100}$, $h=\frac{1}{14}$, $T=0.2$, $k=0.01$ and grid size 15×15.

Table 2. u and v for example 1 at $\epsilon=\frac{1}{500}$, $h=\frac{1}{20}$, $T=2$, $k=0.01$ and grid size 21×21

	u				v			
Mesh point	Literature [15]	LSGrFEM	Exact solution	Pointwise errors of LSGrFEM $\|u-u_h\|$	Literature [15]	LSGrFEM	Exact solution	Pointwise errors of LSGrFEM $\|v-v_h\|$
$(0.1,0.1)$	0.49729	0.50009	0.50000	$9.950e^{-05}$	1.00271	0.99990	0.99999	$9.950e^{-05}$
$(0.5,0.1)$	0.50024	0.50000	0.50000	$3.474e^{-07}$	0.99976	0.99999	1	$3.474e^{-07}$
$(0.9,0.1)$	0.49934	0.49999	0.50000	$3.388e^{-08}$	1.00066	1	1	$3.388e^{-08}$
$(0.3,0.3)$	0.50690	0.50007	0.50000	$7.508e^{-05}$	0.99310	0.99992	0.99999	$7.508e^{-05}$
$(0.7,0.3)$	0.49928	0.49999	0.50000	$3.388e^{-08}$	1.00072	1	1	$3.388e^{-08}$
$(0.1,0.5)$	0.43939	0.50850	0.50048	$8.0e^{-03}$	1.06061	0.99150	0.99952	$8.0e^{-03}$
$(0.5,0.5)$	0.49951	0.50010	0.50000	$1.078e^{-04}$	1.00049	0.99989	0.99999	$1.078e^{-04}$
$(0.9,0.5)$	0.51355	0.49999	0.50000	$1.250e^{-06}$	0.98646	1	1	$1.250e^{-06}$
$(0.3,0.7)$	0.41647	0.51229	0.50048	$1.18e^{-02}$	1.08353	0.98770	0.99952	$1.18e^{-02}$
$(0.7,0.7)$	0.51008	0.49984	0.50000	$1.604e^{-04}$	0.98992	1.00016	0.99999	$1.604e^{-04}$
$(0.1,0.9)$	0.75004	0.74988	0.74999	$1.161e^{-04}$	0.74996	0.75011	0.75000	$1.161e^{-04}$
$(0.5,0.9)$	0.42909	0.49532	0.50048	$5.0e^{-03}$	1.07091	1.00468	0.99952	$5.0e^{-03}$
$(0.9,0.9)$	0.56275	0.49999	0.50000	$7.116e^{-06}$	0.93725	1	0.99999	$7.116e^{-06}$

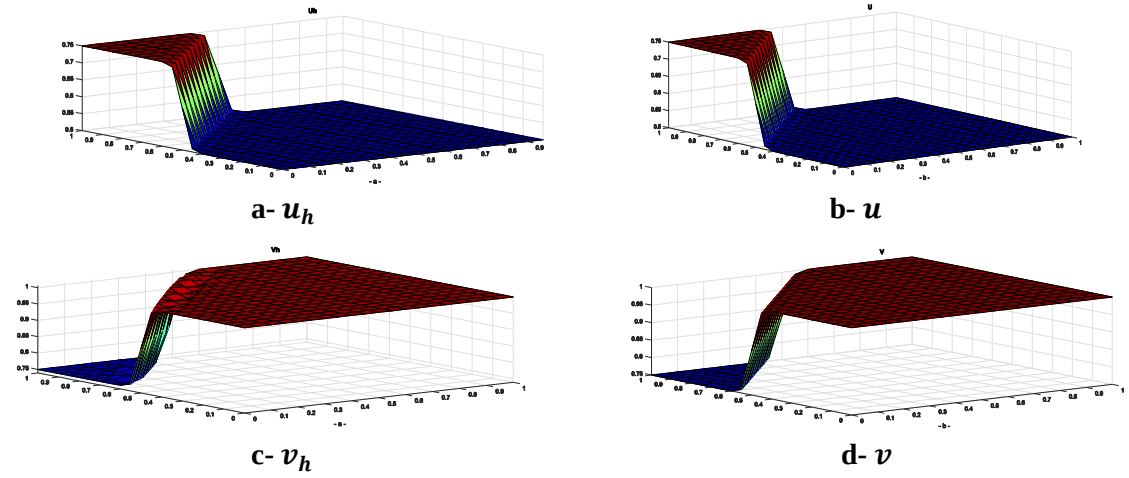

a- u_h b- u

c- v_h d- v

Figure 3. Numerical solutions of LSGrFEM and exact solutions of u and v respectively at $\epsilon=\frac{1}{500}$, $h = \frac{1}{20}$, $T = 2$, $k = 0.01$ and grid size 21×21.

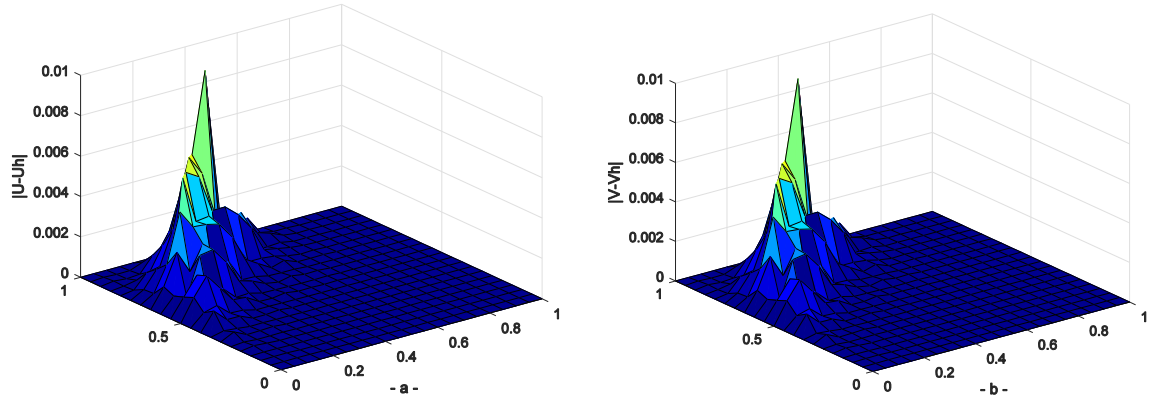

Figure 4. Pointwise errors of LSGrFEM for a.$|u - u_h|$ and b.$|v - v_h|$ respectively at $\epsilon=\frac{1}{500}$, $h = \frac{1}{20}$, $T = 2$, $k = 0.01$ and grid size 21×21.

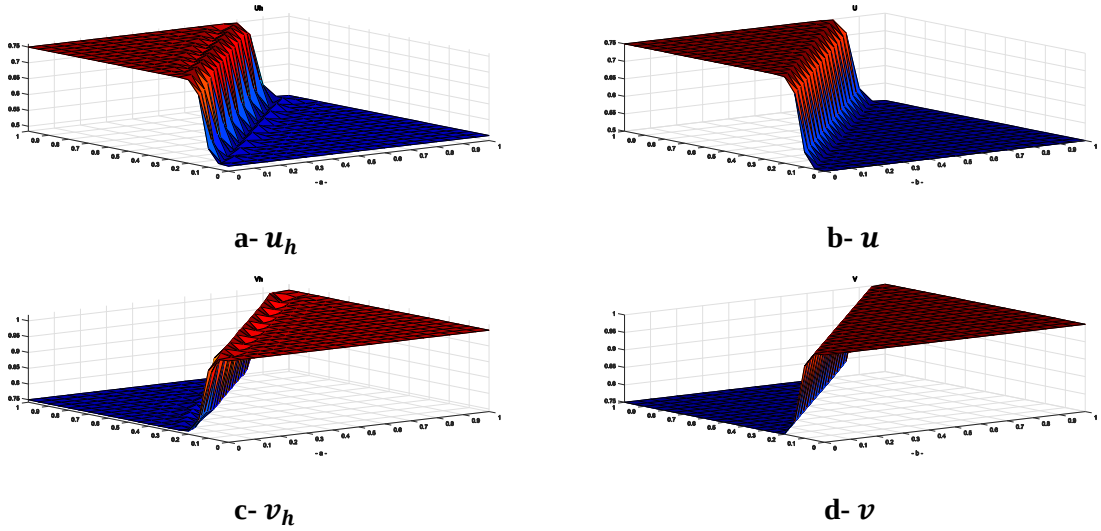

a- u_h b- u

c- v_h d- v

Figure 5. Numerical solutions of LSGrFEM and exact solutions of u and v respectively at $\epsilon=\frac{1}{500}$, $h = \frac{1}{20}$, $T = 0.5$, $k = 0.01$ and grid size 21×21.

Example 2. In this example, a LSGrFEM 25 - 26 over the domain $\bar{\Omega} = [0, 0.5] \times [0, 0.5]$ is constructed . This example has been considered in literature [16]. In Tabs. 3-4, the numerical solutions for various nodes of the grid at $\epsilon = \frac{1}{100}$, $h = \frac{0.5}{20}$, $T = 0.4$, $k = 0.0001$ and grid size 21×21 are computed, in tabular illustrations, the exact solutions and the solutions available in literature [16] are mentioned to compare with our numerical results. It can be seen that the LSGrFEM performed better results and agree with exact solutions than that obtained by literature [16], for which the exact solution is given as,

$$u(x, y, t) = \frac{x + y - 2xt}{1 - 2t^2}, \quad v(x, y, t) = \frac{x - y - 2yt}{1 - 2t^2} .$$

The numerical results have been depicted in Figs. 6-7. From tabular illustrations and numerical results, note that, our method gives better results and produces stable solutions than those suggested in literature [16].

Table 3. u for example 2 at $\epsilon = \frac{1}{100}$, $h = \frac{0.5}{20}$, $T = 0.4$, $k = 0.0001$ and grid size 21×21

Mesh point	u			
	Literature [16]	LSGrFEM	Exact solution	Pointwise errors of LSGrFEM $\lvert u - u_h \rvert$
$(0.1, 0.1)$	0.1764702762	0.17647058824	0.17647058823	$5.6662e^{-12}$
$(0.3, 0.1)$	0.2352911765	0.23529411764	0.23529411764	$1.8318e^{-12}$
$(0.2, 0.2)$	0.3529400063	0.35294117647	0.35294117647	$5.9327e^{-12}$
$(0.4, 0.4)$	0.4117610685	0.41176470588	0.41176470588	$4.4164e^{-13}$
$(0.1, 0.3)$	0.4705813725	0.47058823529	0.47058823529	$3.1618e^{-12}$
$(0.3, 0.3)$	0.5294129028	0.52941176470	0.52941176470	$4.8350e^{-13}$
$(0.2, 0.4)$	0.6470514764	0.64705882353	0.64705882352	$1.2215e^{-12}$
$(0.3, 0.4)$	0.6764723529	0.67647058823	0.67647058823	$9.8587e^{-14}$
$(0.5, 0.5)$	0.8823524117	0.88235294117	0.88235294117	0

Table 4. v for example 2 at $\epsilon = \frac{1}{100}$, $h = \frac{0.5}{20}$, $T = 0.4$, $k = 0.0001$ and grid size 21×21

Mesh point	v			
	Literature [16]	LSGrFEM	Exact solution	Pointwise errors of LSGrFEM $\lvert v - v_h \rvert$
$(0.1, 0.1)$	-0.1176411207	-0.11764705882	-0.11764705882	$1.5403e^{-12}$
$(0.3, 0.1)$	0.1764703671	0.17647058823	0.17647058823	$4.8955e^{-13}$
$(0.2, 0.2)$	-0.2352935294	-0.23529411765	-0.23529411764	$5.8641e^{-12}$
$(0.4, 0.4)$	0.0588233151	0.058823529410	0.058823529411	$5.7026e^{-13}$
$(0.1, 0.3)$	-0.6470530484	-0.64705882353	-0.64705882352	$4.0228e^{-12}$
$(0.3, 0.3)$	-0.3529405402	-0.35294117647	-0.35294117647	$1.9322e^{-12}$
$(0.2, 0.4)$	-0.7647033151	-0.76470588235	-0.76470588235	$2.1446e^{-12}$
$(0.3, 0.4)$	-0.6176410485	-0.61764705882	-0.61764705882	$1.2788e^{-12}$
$(0.5, 0.5)$	-0.5882311745	-0.58823529411	-0.58823529411	0

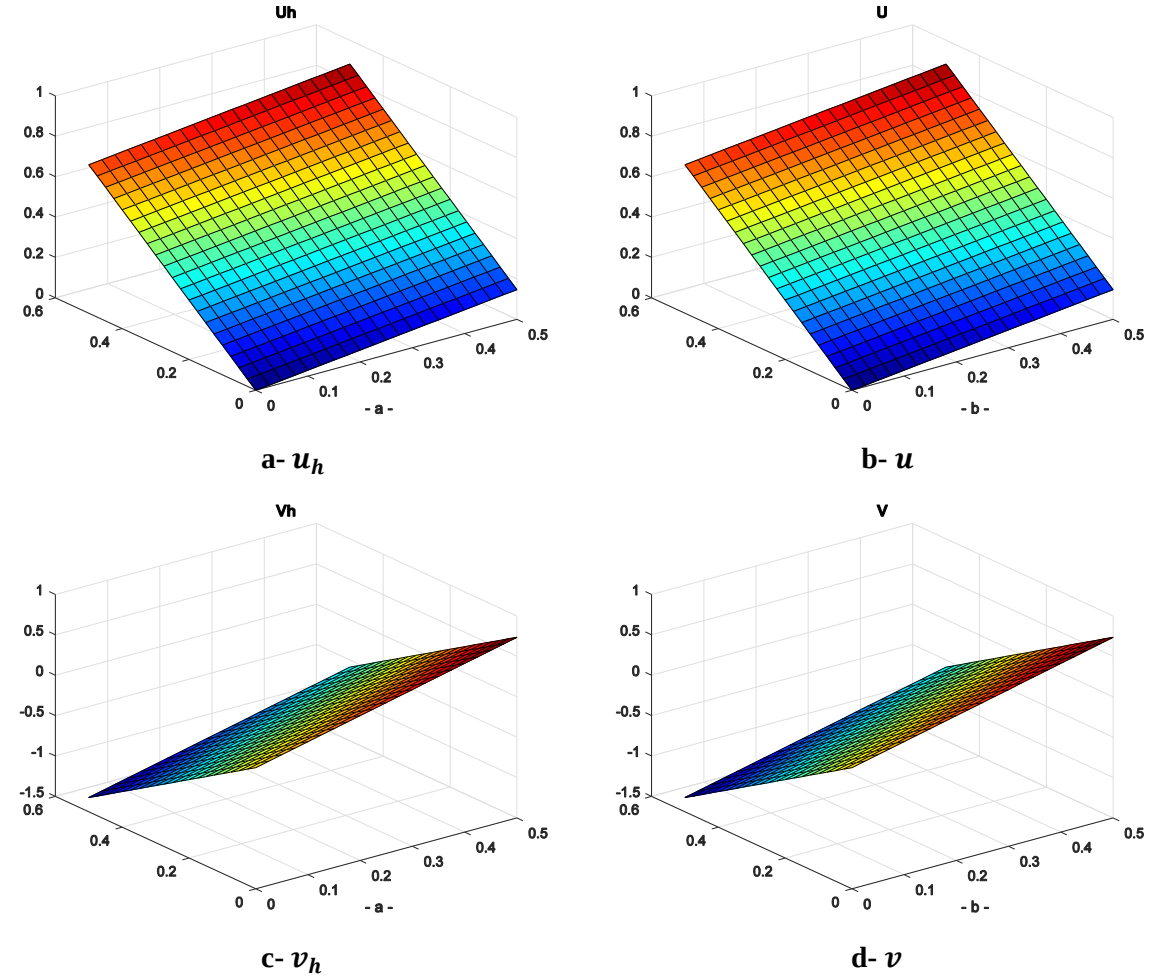

a- u_h b- u

c- v_h d- v

Figure 6. Numerical solutions of LSGrFEM and exact solutions of u and v respectively at ϵ=$\frac{1}{100}$, $h = \frac{0.5}{20}$, $T = 0.4$, $k = 0.0001$ and grid size 21×21 .

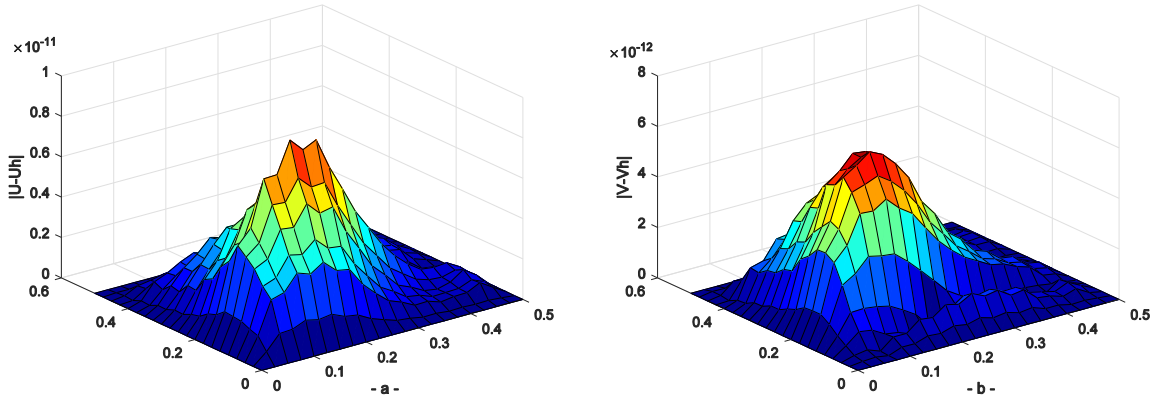

Figure 7. Pointwise errors of LSGrFEM for a. $|u - u_h|$ and b $|v - v_h|$ respectively at ϵ=$\frac{1}{100}$, $h = \frac{0.5}{20}$, $T = 0.4$, $k = 0.0001$ and grid size 21×21 .

Example 3. In this example the computational domain has been taken as $\bar{\Omega} = [0,1] \times [0,1]$, a LSGrFEM 25 – 26 is constructed. This example has been considered in literature [17]. In Tabs 5-6 the numerical solutions at ϵ=$\frac{1}{500}$, $h = \frac{1}{20}$, $T = 0.5$, $k = 0.001$ and grid size 21×21 are computed, in tabular illustrations, our numerical results with the exact solutions and the solutions available in literature [17] are compared for various nodes of the grid. The tabulated results show that LSGrFEM

produces better result than literature [17], where the exact solution are given as,

$$u(x,y,t) = \frac{-4\pi\epsilon e^{-5\epsilon\pi^2 t}\, cos(2\pi x) sin(\pi y)}{2 + e^{-5\epsilon\pi^2 t} sin(2\pi x)\, sin(\pi y)},$$

$$v(x,y,t) = \frac{-2\pi\epsilon e^{-5\epsilon\pi^2 t}\, sn(2\pi x) cos(\pi y)}{2 + e^{-5\epsilon\pi^2 t} sin(2\pi x)\, sin(\pi y)}.$$

Numerical results have been depicted in Figs. 8-9, moreover, at at $\epsilon=\frac{1}{1000}$, $h = \frac{1}{20}$, $T = 1$ and $k = 0.01$, the numerical solutions are calculated and compared with the exact solution as illustrated in Figs. 10-11. From tabular illustrations and numerical results, again note that, our method gives better results and produces stable solutions than those suggested in literature [17].

Table 5. u and v for example 3 at $\epsilon=\frac{1}{500}$, $h = \frac{1}{20}$, $T = 0.5$ and $k = 0.001$ and grid size 21×21

	u			
Mesh point	Literature [17]	LSGrFEM	Exact solution	Pointwise errors of LSGrFEM $\lvert u - u_h \rvert$
$(0.1, 0.1)$	-0.0025582	-0.0027507	-0.0027523	$1.5955e^{-06}$
$(0.5, 0.1)$	0.0031558	0.0037214	0.0036962	$2.5183e^{-05}$
$(0.9, 0.1)$	-0.0045862	-0.0033040	-0.0032732	$3.0812e^{-05}$
$(0.3, 0.3)$	0.0025505	0.0021680	0.0021888	$2.0724e^{-05}$
$(0.7, 0.3)$	0.0048155	0.0050170	0.0047179	$2.9905e^{-04}$
$(0.1, 0.5)$	-0.0079932	-0.0075033	-0.0075615	$5.8239e^{-05}$
$(0.5, 0.5)$	0.0111522	0.0118783	0.0119612	$8.2936e^{-05}$
$(0.3, 0.7)$	0.0025201	0.0021680	0.0021888	$2.0724e^{-05}$
$(0.7, 0.7)$	0.0046522	0.0050170	0.0047179	$2.9904e^{-04}$
$(0.1, 0.9)$	-0.0028582	-0.0027507	-0.0027523	$1.5955e^{-06}$
$(0.5, 0.9)$	0.0032560	0.0037214	0.0036962	$2.5183e^{-05}$
$(0.9, 0.9)$	-0.0038475	-0.0033040	-0.0032732	$3.0812e^{-05}$

Table 6. v for example 3 at $\epsilon=\frac{1}{500}$, $h = \frac{1}{20}$, $T = 0.5$ and $k = 0.001$ and grid size 21×21

	v			
Mesh point	Literature [17]	LSGrFEM	Exact solution	Pointwise errors of LSGrFEM $\lvert v - v_h \rvert$
$(0.1, 0.1)$	-0.0032295	-0.0030892	-0.0030772	$1.5955e^{-06}$
$(0.5, 0.1)$	0.0002448	$-3.703889e^{-16}$	$-6.965711e^{-19}$	$2.5183e^{-05}$
$(0.9, 0.1)$	0.0038201	0.0036669	0.0036596	$3.0812e^{-05}$
$(0.3, 0.3)$	-0.0025507	-0.0024402	-0.0024471	$6.8874e^{-06}$
$(0.7, 0.3)$	0.0052798	0.0054104	0.0054748	$1.3559e^{-04}$
$(0.1, 0.5)$	0.0001158	$4.256802e^{-17}$	$-1.681998e^{-19}$	$5.8239e^{-05}$
$(0.5, 0.5)$	0.0002052	$-2.029357e^{-30}$	$-4.484768e^{-35}$	$8.2936e^{-05}$
$(0.3, 0.7)$	0.0022758	0.0024402	0.0024471	$6.8874e^{-06}$
$(0.7, 0.7)$	-0.0054471	-0.0054104	-0.0052748	$2.9904e^{-04}$
$(0.1, 0.9)$	0.0035521	0.0030892	0.0030772	$1.5955e^{-06}$
$(0.5, 0.9)$	0.0004122	$3.7038892e^{-16}$	$6.9657113e^{-19}$	$2.5183e^{-05}$
$(0.9, 0.9)$	-0.0035518	-0.0036669	-0.0036596	$3.0812e^{-05}$

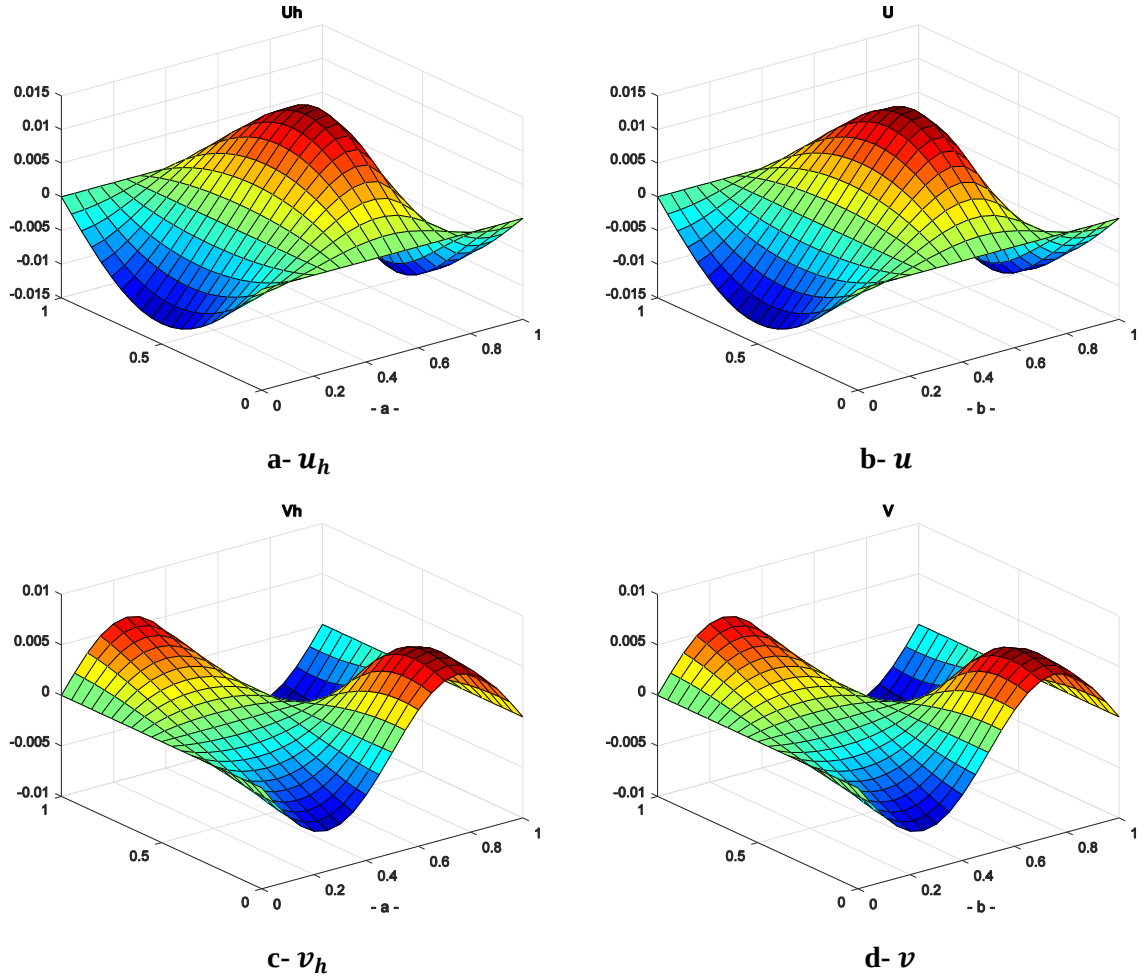

a- u_h b- u

c- v_h d- v

Figure 8. Numerical solutions of LSGrFEM and exact solutions of u and v respectively at ϵ=$\frac{1}{500}$, $h = \frac{1}{20}$, $T = 0.5$ and $k = 0.001$ and grid size 21×21 .

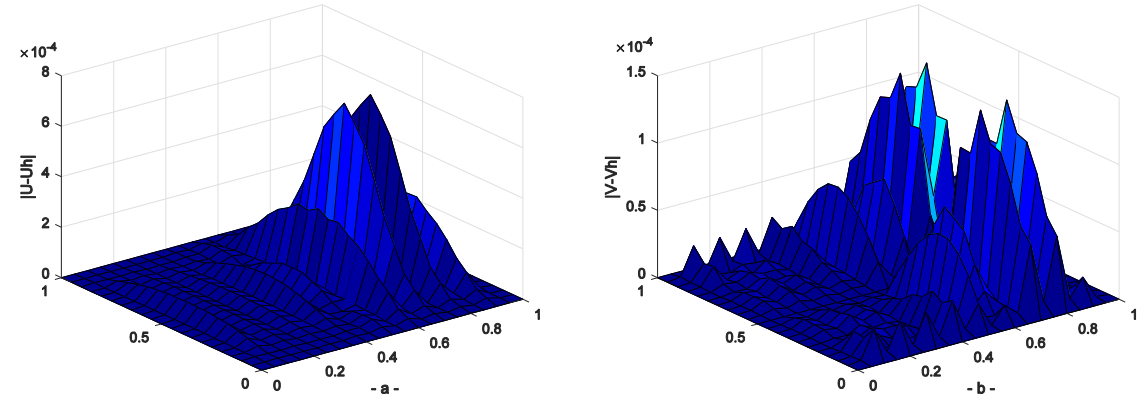

Figure 9. Pointwise errors of LSGrFEM for a.$|u - u_h|$ and b. $|v - v_h|$ respectively at ϵ=$\frac{1}{500}$, $h = \frac{1}{20}$, $T = 0.5$ and $k = 0.001$ and grid size 21×21 .

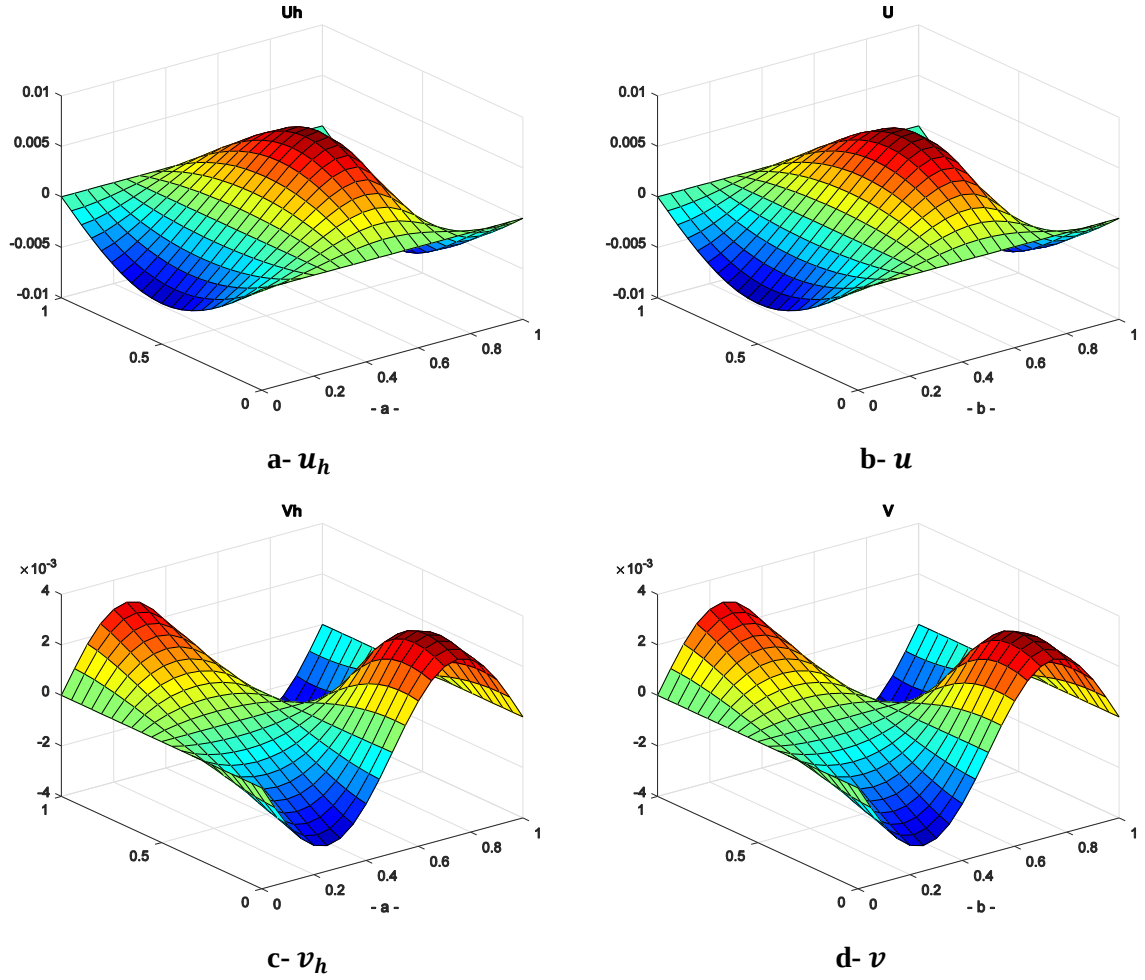

a- u_h b- u

c- v_h d- v

Figure 10. Numerical solutions of LSGrFEM and exact solutions of$u$ and v respectively at ϵ=$\frac{1}{1000}$, $h = \frac{1}{20}, T = 1$ and $k = 0.001$ and grid size 21×21 .

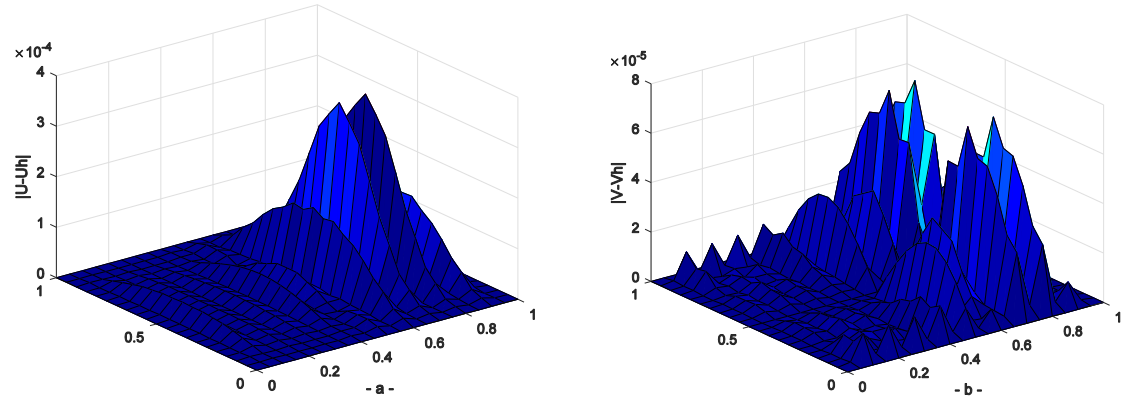

Figure 11. Pointwise errors of LSGrFEM for a.$|u - u_h|$ and b. $|v - v_h|$ respectively at ϵ=$\frac{1}{1000}$, $h = \frac{1}{20}$, $T = 1$ and $k = 0.001$ and grid size 21×21 .

Conclusions:

In this work, the LSGrFEM for 2-D coupled Burgers' problem in the fully discrete case using the backward-Euler scheme for the time variable is considered. From the theoretical analysis and the numerical results, the following conclusions are found:

The continuity and ellipticity of the least-squares functional $\mathcal{F}_1(\varphi, 0)$and $\mathcal{F}_2(\psi, 0)$ are satisfied. The stability condition of LSGrFEM is satisfied. Theoretical analysis show that the error estimate of LSGrFEM is $O(h^r)$. The numerical solution has been compared with the exact solution and other available solutions when the convection-dominated

case. The LSGrFEM is concluded that it provides convergent and consistency approximations in different cases. The results obtained are satisfactory and competent more than the results available in the literature. The LSGrFEM successfully provides accurate solutions and removed all oscillations that occur when ($\epsilon << h$), moreover, the LSGrFEM is suitable to deal with other nonlinear partial differential equations at high Reynolds number.

Authors' declaration:

- Conflicts of Interest: None.
- I hereby confirm that all the Figures and Tables in the manuscript are mine. Besides, the Figures and images, which are not mine ours, have been given the permission for re-publication attached with the manuscript.
- The author has signed an animal welfare statement.
- Ethical Clearance: The project was approved by the local ethical committee in the ministry of education-general directorate of Basrah education.

Authors' contributions:

The author contributed to the design and implementation of the research, to the analysis of the results and to the writing of the manuscript

References:

1. Hussin C H C, Azmi A, Ismail A I M, Kilicman A. Approximate Analytical Solutions of Bright Optical Soliton for Nonlinear Schrödinger Equation of Power Law Nonlinearity, Baghdad Sci J., 2021; 18 (1), 836-845.
2. Aswhad A A. Approximate Solution of Delay Differential Equations Using the Collocation Method Based on Bernstien Polynomials, Baghdad Sci J., 2011; 8(3), 820-825.
3. Barbara F S, Roberta V G, Paula C P, Romao E C. Interval study of convergence in the solution of 1D Burgers by least squares finite element method (LSFEM) + Newton linearization, Sci. Res. Essays, 2015; 10(16), 522-530.
4. Konzen P H A, Azevedo F S, Sauter E, Zingano P R A. Numerical simulations with the galerkin least squares finite element method for the Burgers' equation on the real line, TEMA (São Carlos) , 2017; 18(2), 287-304.
5. Ye X, Zhang S, A discontinuous least-squares finite-element method for second-order elliptic equations, Int. J. Comput. Math., 2018; ISSN: 1029-0265, 1-11.
6. Kalchev D Z, Manteuffel T A, Münzenmaier S. Mixed $(\mathcal{L}\mathcal{L}^*)^{-1}$ and $\mathcal{L}\mathcal{L}^*$ least-squares finite element methods with application to linear hyperbolic problems. Numer. Linear Algebra Appl., 2018; special issue paper, 1-24.
7. Barrenechea G R, Knobloch P. Analysis of a group finite element formulation, Appl Numer Math., 2017; (18), 238–248.
8. Benosman M, Kramer B, Boufounos P T, Grover P. Learning-based Reduced Order Model Stabilization for Partial Differential Equations: Application to the Coupled Burgers' Equation, American Cont. Conf., 2016; 1673-1678.
9. Noon N J. Weak Galerkin and Weak Group Finite Element Methods for 2-D Burgers' Problem, J Adv Res. Fluid Mech and Therm Sci ., 2020; 69(2), 42-59.
10. Fletcher C A J. Computational Techniques for Fluid Dynamics I, Springer-Verlag, 1991; 2^{th} , ch.10, pp.360.
11. Cai Z, Manteuffel T A , Mccormick S F. First-order system least squares for velocity–vorticity–pressure form of the Stokes equations, with application to linear elasticity, Electron. Trans. Numer. Anal. , 1995; 3, 150–159.
12. Larson M G, Bengzon F. The finite element method: theory, implementation and applications, Texts in Computational Science and Engineering, Verlag Berlin Heidelberg, 2013; ISSN 1611-0994, 1^{th}, ch.1, pp.6.
13. Ching L C, Yang S Y. Analysis of the $[L^2,L^2,L^2]$ least-squares finite element method for incompressible Oseen- type problems, Int. J. Numer. Anl. Mod., 2007; 4(3-4), (402-424)
14. Liew S C, Yeak S H. Multiscale Element-Free Galerkin Method with Penalty for 2D Burgers' Equation, J Teknol. (Sci & Eng), 2013; 62(3), 49-56.
15. Srivastava V K, Tamsir M, Bhardwaj U, Sanyasiraju Y. Crank-Nicolson scheme for numerical solutions of two-dimensional coupled Burgers' equations, JSER, 2011; 2 (5), 1-7.
16. Mittal R C, Tripathi A. Numerical solutions of two-dimensional Burgers' equations using modified Bi-cubic B-spline finite elements, Eng. Comput., 2015; 32 (5), 1275 -1306.
17. Kaennakham S, Chuathong N. A Proposed Adaptive Inverse Multiquadric Shape Parameter Applied with the Dual Reciprocity BEM to Nonlinear and Coupled PDE, J.Appl. Sci. , 2017; 17(10), 491-501.

Open Access **Baghdad Science Journal** **P-ISSN: 2078-8665**
2021, 18(4) Supplement: 1521-1535 **E-ISSN: 2411-7986**

التحليل العددي لطريقة المربعات الصغرى للعناصر المحددة المجمعة لمسألة برغرز الثنائية

نجاة جليل نون

قسم الرياضيات، كلية التربية للعلوم الصرفة، جامعة البصرة.

الخلاصة:

في هذا البحث ، قُدمت طريقة المربعات الصغرى للعناصر المحددة المجمعة لحل مسألة برغرز الثنائية ذات البعدين. أستُخدمت صيغة التقطيع الكلي لطريقة المربعات الصغرى للعناصر المحددة المجمعة بتطبيق طريقة اويلر الخلفية لمتغير الزمن ، التقسيم بمتغير الفضاء طُبق كعناصرتربيعية رباعية الزوايا ذات تسع عقد لكل عنصر. تم إثبات الاستمرارية والإهليلجية وشرط الاستقرار وتقدير الخطأ لطريقة المربعات الصغرى للعناصر المحددة المجمعة ، حيث بينت النتائج النظرية ان تقدير الخطأ لهذه الطريقة هو . o(h^r)تم مقارنة النتائج العددية مع الحل الدقيق والأبحاث الأخرى المتاحة عندما تكون الحالة التي يسيطر عليها الحمل الحراري لتوضيح كفاءة الطريقة المقترحة حيث تم حلها من خلال التنفيذ في برنامج ماتلاب 2018.

الكلمات المفتاحية: مسألة برغرز، طريقة العناصر المحدودة المجمعة، مربعات صغرى.